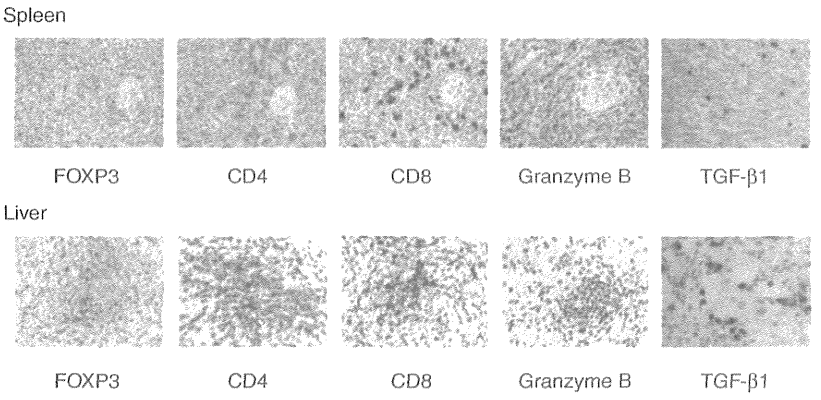

Figure 1 Immunohistochemical staining of spleen and liver specimens with forkhead box P3 (FOXP3), CD4, CD8, granzyme B and transforming growth factor (TGF)-β1 in the spleen and liver.

lymphocytes, $CD8^+$ lymphocytes, FOXP3, granzyme B and TGF-β1 positive cells (Fig. 1). We classified liver specimens into five stages according to the degree of fibrosis as follows: F0, no fibrosis in the portal tract; F1, portal fibrosis without septa; F2, portal fibrosis with a few septa; F3, numerous septa without cirrhosis; and F4, cirrhosis. We collected resected liver specimens from 10 cases each of F1, F2, F3 and F4 with HCV-related liver disease. We also collected specimens from eight cases of liver hemangioma of F0 with both negative hepatitis B surface antigen and HCV antibody. Follow-up liver biopsy sections were obtained from the same part of the liver if possible from seven of the 26 patients at various intervals after splenectomy (Table 2). These sections were used for CD4 and CD8 immunostaining and Masson-trichrome staining for the morphometric evaluation of fibrotic areas.

Spleen tissue

A total of 26 spleens with HCV-related liver cirrhosis and hypersplenism were examined for the immunohistochemical expression of CD4 positive lymphocytes, CD8 positive lymphocytes, FOXP3, granzyme B and TGF-β1 positive cells. We measured the same parameters in spleens from the seven control cases in control group 3 as a non-cirrhotic control (Fig. 1). Spleen and liver tissues were pathologically assessed by two pathologists (Y. N. and M. K.).

Peripheral blood cells

Peripheral blood samples were serially collected from 26 patients with HCV-related liver cirrhosis and hypersplenism just before and 14 days, 1 month, 3 months, 6 months and 1 year after splenectomy. We examined the ratio of $CD4^+$ T cells to all lymphocytes, $CD8^+$ T cells to all lymphocytes, and the $CD4^+/CD8^+$ ratio in PB samples using flow cytometry. TGF-β1 levels in PB were also measured using enzyme-linked immunoassays in the sera just before and 14 days, 1 month, 3 months, 6 months and 1 year after splenectomy. Patients were excluded from the protocol if IFN or other therapeutics were introduced for the liver disease. Ten healthy adult

Table 2 Clinical and pathological findings of 7 patients who underwent follow-up liver biopsies

Case	Age	Sex	Activity	Child–Pugh (score)	CD4/8	Follow-up range (days)	Before (%)	After (%)	Rate of change
1	63	M	1	A (5)	1.73	581	6.59	18.31	2.78
2	58	M	2	A (5)	1.22	24	7.38	8.99	1.22
3	58	M	2	B (7)	1.57	333	9.92	12.02	1.21
4	52	M	2	A (5)	1.08	431	16.71	5.10	0.30
5	74	M	2	A (6)	0.63	353	20.02	6.31	0.32
6	53	F	2	A (6)	0.93	248	30.03	13.34	0.44
7	59	M	2	A (5)	0.95	42	11.27	8.05	0.71

Activity: A0, none; A1, portal inflammation only; A2, mild interface hepatitis; A3, moderate interface hepatitis; A4, severe interface hepatitis.
Before, the rate of fibrotic areas before splenectomy; after, the rate of fibrotic areas after splenectomy.

volunteers in control group 2 without a history of liver disease or splenomegaly were also recruited as controls, and samples were collected only once.

Immunohistochemical analysis

All fresh specimens were fixed by 10% formalin, and paraffin-embedded tissue samples were cut at a thickness of 4 μm, examined on a coated slide glass, and labeled with the following antibodies using the Bond-Max autostainer (Leica Microsystems, Newcastle, UK) and DAKO autostainer (DakoCytomation, Glostrup, Denmark): CD4 (×200; Leica Microsystems), CD8 (×200; Leica Microsystems), granzyme B (×50; Leica Microsystems), TGF-β1 (×300; Santa Cruz Biotechnology, Heidelberg, Germany) and FOXP3 (×600; Abcam, Cambridge, MA, USA).

Immunohistochemical examinations with CD4, CD8, granzyme B and TGF-β1 were performed on the same fully automated Bond-Max system using onboard heat-induced antigen retrieval with ER2 for 10 min and the Refine polymer detection system (Leica Microsystems). 3,3′-Diaminobenzidine-tetrachloride (DAB) was used as the chromogen for all immunostaining. FOXP3 immunostaining was carried out using the DAKO autostainer with the ChemMate ENVISION method (DakoCytomation). Briefly, specimens were boiled in a microwave for 30 min in 1 mmol/L ethylenediaminetetraacetic acid, pH 9.0, and target retrieval solution (DakoCytomation) to recover antigens, and the specimens were then incubated with the antibody at 4°C overnight. After washing in Tris-buffered saline (TBS), slides were incubated with the labeled polymer-horseradish peroxidase secondary antibody for 30 min at room temperature. After washing in TBS, slides were visualized using DAB.

Detection of immune function using flow cytometry

T-lymphocyte subsets in PB such as CD4, CD8 and CD4/8 were determined by flow cytometry, and the monoclonal antibodies of CD4 and CD8 (labeled CD4-FITC, CD-8-RD1) were purchased from Beckman Coulter (Danvers, MA, USA).

Result assessment

For assessment criteria for lymphocytes and other positive cell counts, the number of lymphocytes and other positive cells were counted in 20 areas within a specimen under high-power fields (×40 objective, ×10 eyepiece). Ten areas of white and red pulp were assessed in the spleen, and 10 periportal areas and 10 hepatic lobule areas (Fig. 1) were assessed in a non-tumor area of the liver.

Morphometric analysis (computer image analysis) was performed in the following manner on specimens stained with Masson-trichrome. The equipment used to assess morphometry consisted of a light microscope, a three-color charge-coupled device camera, and a high resolution computer image analysis system (WinRooF software package version 6.1; Mitani, Fukui, Japan). The magnified images (×40) of specimens captured by the camera mounted on the microscope were sent to the image analyzing computer. Collagen fibers stained with Masson-trichrome were then selected. In this study, this scanning procedure was repeated 10 times in random areas. The area of fibrosis (AF) was defined as the ratio (%) of the whole area of collagen fibers to that of the liver tissue scanned.

Statistical analyses

Statistical analysis was performed using Student's *t*-test. A *P*-value of less than 0.05 was considered to be significant.

The follow-up time was calculated as the interval between the date of surgery and intervention of the medical treatment, last follow up or recognition of HCC. Survival rates or failure rates were analyzed with the Kaplan–Meier method using the log-rank test to assess differences between curves. A *P*-value of less than 0.05 was considered to be significant. Statistical calculations were performed using the JMP software package (release 10, SAS Institute, Cary, NC, USA).

RESULTS

Liver

IN THE SEVEN follow-up liver biopsy sections (Table 2) available for histological examination, liver fibrosis in the hepatic lobules improved from F4 to F3 in four cases (cases 4–7: average, 268.5 ± 168.6 days; range, 42–431 days) (Fig. 2a). Improvements were not observed in the remaining three cases (cases 1–3: average, 312 ± 279.1 days; range, 24–581 days) (Fig. 2b). There were no statistical differences in the duration between the improvement cases and non-improvement cases ($P = 0.80$). Conducting an evaluation was difficult because only a few specimens were available; however, no significant differences in clinical profiles were observed among the seven patients. In four of these cases (cases 4–7), the ratio significantly

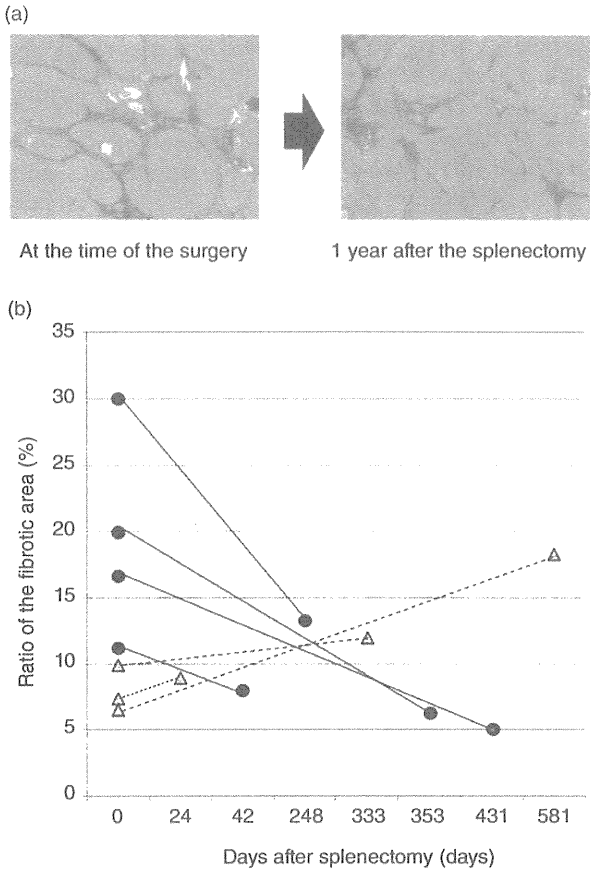

Figure 2 (a) Improvements in liver fibrosis. Distortions in hepatic lobules improved in the liver biopsy sections of four cases after splenectomy, and fibrotic areas significantly decreased from 19.5% to 8.2% in these sections. (b) Changes in the fibrotic areas of seven patients at various intervals. •—• shows patients in whom the fibrotic area significantly decreased after splenectomy. △···△ shows patients in whom fibrosis deteriorated.

decreased from 19.5% to 8.2% ($P < 0.05$) (Fig. 2b), while the average AF in the remaining three cases (cases 1–3) increased from 8.0% to 13.1% ($P = 0.15$). The four cases of improved fibrosis were all Child–Pugh A, and one of the three cases that showed no improvement was Child–Pugh B. In addition, AF before splenectomy was slightly higher in the improvement cases than in the non-improvement cases, while the $CD4^+/CD8^+$ ratio before splenectomy was lower in the improvement cases than in the non-improvement cases ($P < 0.05$). Histopathologically, $CD4^+$ and $CD8^+$ lymphocytes were mainly seen in the periportal area, and $CD4^+$ lymphocytes were rarely seen in the hepatic lobules. The epithelial cells, fibroblasts, monocytes and macrophages also produced TGF-β1.[4,21,26] However, we picked up and counted the TGF-β1 positive cells that were seen in the lymphocytes and found that these cells were distributed diffusely in the hepatic lobules and periportal area. The distribution pattern of Treg and granzyme B was the same as that of $CD4^+$ and $CD8^+$ lymphocytes, respectively. No significant differences were observed in the $CD4^+/CD8^+$ ratio ($P = 0.21$) in liver specimens, regardless of the association of HCC. The $CD4^+/CD8^+$ ratio ($P < 0.05$) and FOXP3/$CD4^+$ ratio ($P < 0.001$) significantly increased with the progression of liver fibrosis (from F0 to F4). However, the granzyme B/$CD8^+$ ratio was approximately constant, and was unrelated to the progression of liver fibrosis ($P = 0.32$).

The number of TGF-β1 positive cells in livers with HCC was slightly higher than that in livers without ($P = 0.06$), and the number of TGF-β1 positive cells also significantly increased with the progression of liver fibrosis ($P < 0.001$) (Fig. 3).

Spleen

Histopathologically, $CD4^+$ and $CD8^+$ lymphocytes were found more in the white pulp than in the red pulp. The results of the clinicopathological analysis showed that the $CD4^+/CD8^+$ ratio in spleens with HCV-related liver cirrhosis and hypersplenism was higher than that in the spleens of control group 3 ($P = 0.06$). The FOXP3/$CD4^+$ ratio in control group 3 was higher than that in cases of hypersplenism ($P < 0.05$), and no significant differences

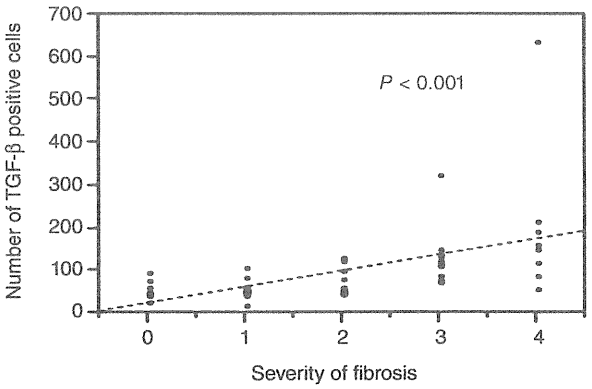

Figure 3 Correlation between transforming growth factor (TGF)-β1 positive cells and fibrosis in the liver. The number of TGF-β1 positive cells also significantly increased with the progression of liver fibrosis.

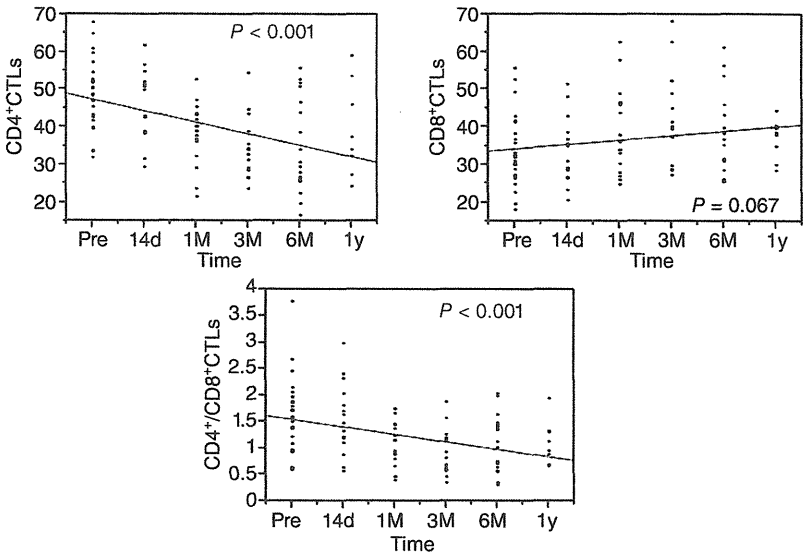

Figure 4 Changes in peripheral blood after splenectomy. pre, preoperative; d, days; M, months; y, year. The ratio of $CD4^+$ T cells to all lymphocytes significantly decreased 1 year after splenectomy, while the ratio of $CD8^+$ T cells to all lymphocytes slightly increased, resulting in a significant decrease in the $CD4^+/CD8^+$ ratio.

in the granzyme B/$CD8^+$ ratio ($P = 0.82$) were observed between the splenectomy group and control group 3 (data not shown).

Peripheral blood

The ratio of $CD4^+$ T cells to all lymphocytes and the $CD4^+/CD8^+$ ratio in PB samples obtained from 26 patients before splenectomy were significantly higher than those from control group 2 ($P < 0.01$, $P < 0.05$). In contrast, the ratio of $CD4^+$ T cells to all lymphocytes significantly decreased 1 year after splenectomy ($P < 0.001$), while the ratio of $CD8^+$ T cells to all lymphocytes slightly increased ($P = 0.07$), resulting in a significant decrease in the $CD4^+/CD8^+$ ratio ($P < 0.001$) (Fig. 4).

Transforming growth factor-β levels were higher in PB samples from patients with HCC than in those without. TGF-β1 levels slightly increased in PB samples 1 month after splenectomy, then decreased, and subsequently returned to the level measured before splenectomy in 1 year.

Relationship of the $CD4^+/CD8^+$ ratio between PB and the spleen or liver

In the splenectomy group, the $CD4^+/CD8^+$ ratio in PB had a significant positive correlation with the $CD4^+/CD8^+$ ratio in the spleen ($P < 0.05$), and was also positively associated with the liver ($P = 0.07$). As a result, a significant positive correlation was observed between the $CD4^+/CD8^+$ ratio in the spleen and that in the liver ($P < 0.05$) (Fig. 5).

Correlation between the $CD4^+/CD8^+$ ratio and clinical prognosis

We compared the $CD4^+/CD8^+$ ratio between PB obtained pre-splenectomy and 1 month after splenectomy ($n = 19$). The median of differences between pre-splenectomy and 1 month after splenectomy was 0.5. The occurrence of HCC was significantly lower in cases in which the difference in the $CD4^+/CD8^+$ ratio between the perioperative period and 1 month later was over 0.5 (≥0.5 vs <0.5, $P < 0.05$) (Fig. 6a).

A positive correlation in PB was observed between the $CD4^+/CD8^+$ ratio before splenectomy and differences in the $CD4^+/CD8^+$ ratio between pre-splenectomy and 1 month after splenectomy ($P < 0.001$). As the median of the preoperative $CD4^+/CD8^+$ ratio was 1.7, the postoperative (1 month after splenectomy) $CD4^+/CD8^+$ ratio significantly decreased in groups in which the preoperative value was larger than 1.7 (Fig. 6b,c).

DISCUSSION

PREVIOUS STUDIES HAVE shown that splenectomy was effective in improving pancytopenia, the decompression of portal hyperpressure and liver function.[1,2,27,28] Morinaga *et al.* reported that splenectomy

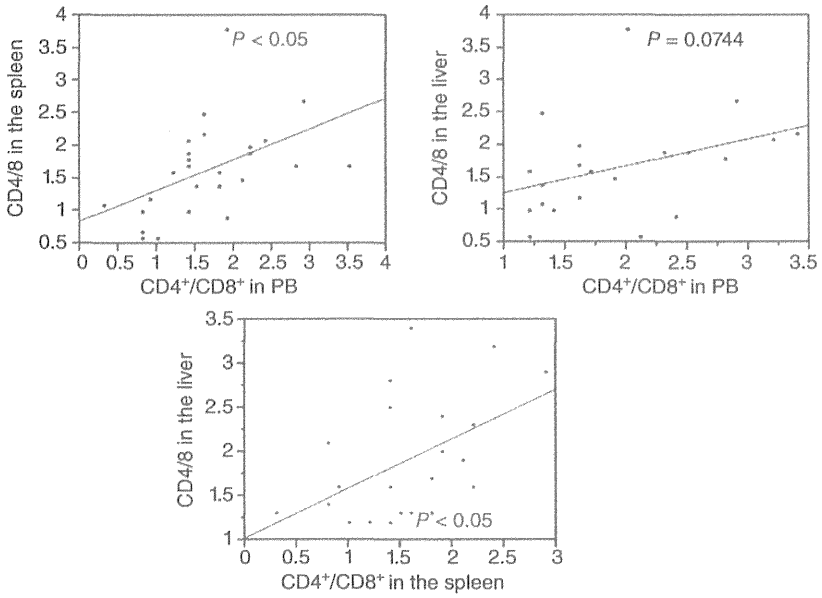

Figure 5 Correlations between the $CD4^+/CD8^+$ ratios in the spleen, liver and peripheral blood (PB). A significant positive correlation was observed between the $CD4^+/CD8^+$ ratio in the spleen and that in the liver.

significantly improved liver fibrosis with a reduction in plasma TGF-β1 levels in the rat. However, all these reports of hepatic fibrosis were conducted in animal models[1,16,29,30] whereas the present study described improvements in liver fibrosis after splenectomy in humans. Interestingly, the $CD4^+/CD8^+$ ratio changed after splenectomy without other treatment. However, many confounding factors may be implicated in this change. It is likely that patients with a high fibrotic area in their liver specimens had a high $CD4^+/CD8^+$ ratio;

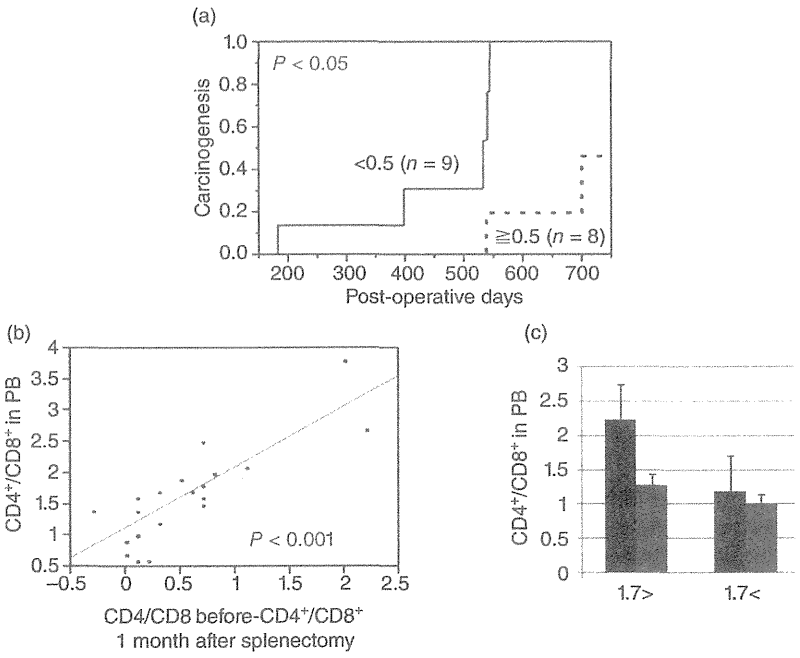

Figure 6 (a) Correlation between carcinogenesis, the perioperative period and 1 month later. The occurrence of hepatocellular carcinoma was significantly lower in cases in which the difference in the $CD4^+/CD8^+$ ratio between the perioperative period and 1 month later was over 0.5. (b,c) Correlation in peripheral blood (PB) between the $CD4^+/CD8^+$ ratio before surgery and differences in the $CD4^+/CD8^+$ ratios before splenectomy and 1 month after splenectomy. (b) A positive correlation in PB was observed between the $CD4^+/CD8^+$ ratio before splenectomy and differences in the $CD4^+/CD8^+$ ratio between pre-splenectomy and 1 month after splenectomy. (c) The postoperative (1 month after splenectomy) $CD4^+/CD8^+$ ratio significantly decreased in groups in which the preoperative value was larger than 1.7. ■, pre; ■, post.

therefore, we may expect a decrease in the $CD4^+/CD8^+$ ratio after splenectomy. A decrease in Treg cells that stimulate TGF-β1 may lead to alleviation of fibrosis.

Because the immune function of $CD4^+$ CTL, $CD8^+$ CTL and the $CD4^+/CD8^+$ ratio is affected by a wide variety of factors including recent exercise, poor nutrition and coincident acute viral infections, it is difficult to evaluate immune function using only $CD4^+$ CTL, $CD8^+$ CTL and the $CD4^+/CD8^+$ ratio. However, in our study, the ratio of $CD4^+$ T cells to all lymphocytes in PB was significantly decreased in cirrhotic patients after splenectomy, while the ratio of $CD8^+$ T cells to all lymphocytes slightly increased, resulting in a significant decrease in the $CD4^+/CD8^+$ ratio. The $CD4^+/CD8^+$ ratios in PB, spleens and livers were significantly higher in patients with hypersplenism and in those in whom liver fibrosis had progressed than in the controls. As a positive correlation was observed between the $CD4^+/CD8^+$ ratios in the spleens, livers and PB, it is possible to expect to predict the immunological state of the liver and spleen from the immunological state of PB. In addition, carcinogenesis was significantly lower in groups in which a large difference in the $CD4^+/CD8^+$ ratio was observed between before and after splenectomy or in those with a high $CD4^+/CD8^+$ ratio before splenectomy though there were few cases that we could observe. The $CD4^+/CD8^+$ ratio is likely to be a key parameter for appropriate tumor-infiltrating lymphocyte function, and was shown to be different in different types of cancer.[2,31–35] Host immune responses to cancer were reported to depend on T lymphocytes, particularly $CD8^+$ lymphocytes.[18,19,24,36–39] An increase in their ratio after splenectomy and the consequent decrease in the $CD4^+/CD8^+$ ratio observed in this study may be a positive change in terms of immunology against HCC. Such a change was particularly marked in patients with a high $CD4^+/CD8^+$ ratio before splenectomy.

In our study, the $CD4^+/CD8^+$ ratio also significantly increased as the fibrosis of non-tumor areas in the liver tissue progressed. These significant differences were observed regardless of the HCC status. Although the cause of these differences is unknown, it appears to depend on the background of histological factors in the liver such as fibrosis. Many studies have investigated the relationship between tumors, Treg and TGF-β.[20–22,25,40] Guo-He *et al.* showed that the expression of TGF-β appeared to be positively correlated with Treg in HCC tissue. The 5-year survival rate was significantly lower in patients with HCC tissues with high Treg cell infiltration than in those with low infiltration.[20,22,36,41] Our study also revealed that Treg cells were positively correlated with TGF-β1 positive cells even in "non-tumor areas" of liver tissue, and that TGF-β1 positive cells were positively correlated with liver fibrosis. There were no significant differences of TGF-β1 before and after splenectomy. The reason for the chronological changes in TGF-β1 levels after splenectomy is unknown because various factors including platelets may be involved in the production of TGF-β1. We also found a slightly higher number of TGF-β1 positive cells in non-tumor areas in the liver tissue of patients with HCC than in those without. Furthermore, the number of TGF-β1 positive cells significantly increased with the progression of liver fibrosis.[4,21,26,42]

In conclusion, splenectomy in cirrhotic patients with hepatitis may be able to improve liver fibrosis, cause beneficial immunological changes and lower the risk of carcinogenesis. It seems necessary to accumulate further cases to establish a convincing conclusion.

ACKNOWLEDGMENTS

THIS STUDY WAS partially supported by a Health and Labor Sciences Research Grant from the Ministry of Health, Labor and Welfare Japan, regarding Research on Intractable Diseases, Portal Hemodynamic Abnormalities.

REFERENCES

1 Sugawara Y, Yamamoto J, Shimada K *et al.* Splenectomy in patients with hepatocellular carcinoma and hypersplenism. *J Am Coll Surg* 2000; **190**: 446–50.
2 Cao ZX, Chen XP, Wu ZD. Changes of immune function in patients with liver cirrhosis after splenectomy combined with resection of hepatocellular carcinoma. *Hepatobiliary Pancreat Dis Int* 2003; **2**: 562–5.
3 Okuno K, Tanaka A, Shigeoka H *et al.* Suppression of T-cell function in gastric cancer patients after total gastrectomy with splenectomy: implications of splenic autotransplantation. *Gastric Cancer* 1999; **2**: 20–5.
4 Hayashi H, Sakai T. Biological significance of local TGF-beta activation in liver diseases. *Front Physiol* 2012; **3**: 12.
5 Oishi T, Terai S, Iwamoto T, Takami T, Yamamoto N, Sakaida I. Splenectomy reduces fibrosis and preneoplastic lesions with increased triglycerides and essential fatty acids in rat liver cirrhosis induced by a choline-deficient L-amino acid-defined diet. *Hepatol Res* 2011; **41**: 463–74.
6 Hirai K, Kawazoe Y, Yamashita K *et al.* Transcatheter partial splenic arterial embolization in patients with hypersplenism: a clinical evaluation as supporting therapy for hepatocellular carcinoma and liver cirrhosis. *Hepatogastroenterology* 1986; **33**: 105–8.

7 Hashimoto N, Shimoda S, Kawanaka H *et al.* Modulation of CD4(+) T cell responses following splenectomy in hepatitis C virus-related liver cirrhosis. *Clin Exp Immunol* 2011; **165**: 243–50.
8 Morris DH, Bullock FD. The importance of the spleen in resistance to infection. *Ann Surg* 1919; **70**: 513–21.
9 Brown EJ, Hosea SW, Frank MM. The role of the spleen in experimental pneumococcal bacteremia. *J Clin Invest* 1981; **67**: 975–82.
10 Looke DF, Runnegar NJ. Splenectomy and sepsis. *Med J Aust* 2012; **196**: 587.
11 Morgan TL, Tomich EB. Overwhelming post-splenectomy infection (OPSI): a case report and review of the literature. *J Emerg Med* 2011; **43**: 758–63.
12 Samimi F, Irish WD, Eghtesad B, Demetris AJ, Starzl TE, Fung JJ. Role of splenectomy in human liver transplantation under modern-day immunosuppression. *Dig Dis Sci* 1998; **43**: 1931–7.
13 Takasu O, Sakamoto T, Kojiro M, Yano H. Analysis of subendothelial leukocyte infiltration in the trabecular veins of septic spleen. *Kurume Med J* 2010; **57**: 9–20.
14 Levi D, Maurino E, Abecasis R *et al.* Splenic hypofunction in cirrhosis is not associated with increased risk for infections. *Eur J Gastroenterol Hepatol* 1996; **8**: 257–60.
15 Akahoshi T, Hashizume M, Tanoue K *et al.* Role of the spleen in liver fibrosis in rats may be mediated by transforming growth factor beta-1. *J Gastroenterol Hepatol* 2002; **17**: 59–65.
16 Morinaga A, Ogata T, Kage M, Kinoshita H, Aoyagi S. Comparison of liver regeneration after a splenectomy and splenic artery ligation in a dimethylnitrosamine-induced cirrhotic rat model. *HPB (Oxford)* 2009; **12**: 22–30.
17 Yao YM, Liu QG, Yang W, Zhang M, Ma QY, Pan CE. Effect of spleen on immune function of rats with liver cancer complicated by liver cirrhosis. *Hepatobiliary Pancreat Dis Int* 2003; **2**: 242–6.
18 Naito Y, Saito K, Shiiba K *et al.* CD8+ T cells infiltrated within cancer cell nests as a prognostic factor in human colorectal cancer. *Cancer Res* 1998; **58**: 3491–4.
19 Wada Y, Nakashima O, Kutami R, Yamamoto O, Kojiro M. Clinicopathological study on hepatocellular carcinoma with lymphocytic infiltration. *Hepatology* 1998; **27**: 407–14.
20 Kretschmer K, Apostolou I, Hawiger D, Khazaie K, Nussenzweig MC, von Boehmer H. Inducing and expanding regulatory T cell populations by foreign antigen. *Nat Immunol* 2005; **6**: 1219–27.
21 Unitt E, Rushbrook SM, Marshall A *et al.* Compromised lymphocytes infiltrate hepatocellular carcinoma: the role of T-regulatory cells. *Hepatology* 2005; **41**: 722–30.
22 Sakaki M, Hiroishi K, Baba T *et al.* Intrahepatic status of regulatory T cells in autoimmune liver diseases and chronic viral hepatitis. *Hepatol Res* 2008; **38**: 354–61.
23 Lin GH, Wang J, Li SH, Xu L, Li SP. Relationship and clinical significance of TGF-beta1 expression with Treg cell infiltration in hepatocellular carcinoma. *Chin J Cancer* 2010; **29**: 403–7.
24 Kobayashi N, Hiraoka N, Yamagami W *et al.* FOXP3+ regulatory T cells affect the development and progression of hepatocarcinogenesis. *Clin Cancer Res* 2007; **13**: 902–11.
25 Sakaguchi S, Yamaguchi T, Nomura T, Ono M. Regulatory T cells and immune tolerance. *Cell* 2008; **133**: 775–87.
26 Sato M, Muragaki Y, Saika S, Roberts AB, Ooshima A. Targeted disruption of TGF-beta1/Smad3 signaling protects against renal tubulointerstitial fibrosis induced by unilateral ureteral obstruction. *J Clin Invest* 2003; **112**: 1486–94.
27 Wu CC, Cheng SB, Ho WM *et al.* Appraisal of concomitant splenectomy in liver resection for hepatocellular carcinoma in cirrhotic patients with hypersplenic thrombocytopenia. *Surgery* 2004; **136**: 660–8.
28 Murata K, Shiraki K, Sugimoto K *et al.* Splenectomy enhances liver regeneration through tumor necrosis factor (TNF)-alpha following dimethylnitrosamine-induced cirrhotic rat model. *Hepatogastroenterology* 2001; **48**: 1022–7.
29 Shimada M, Hashizume M, Shirabe K, Takenaka K, Sugimachi K. A new surgical strategy for cirrhotic patients with hepatocellular carcinoma and hypersplenism. Performing a hepatectomy after a laparoscopic splenectomy. *Surg Endosc* 2000; **14**: 127–30.
30 Nakamura T, Sakata R, Ueno T, Sata M, Ueno H. Inhibition of transforming growth factor beta prevents progression of liver fibrosis and enhances hepatocyte regeneration in dimethylnitrosamine-treated rats. *Hepatology* 2000; **32**: 247–55.
31 Toes RE, Ossendorp F, Offringa R, Melief CJ. CD4 T cells and their role in antitumor immune responses. *J Exp Med* 1999; **189**: 753–6.
32 Shah W, Yan X, Jing L, Zhou Y, Chen H, Wang Y. A reversed CD4/CD8 ratio of tumor-infiltrating lymphocytes and a high percentage of CD4(+)FOXP3(+) regulatory T cells are significantly associated with clinical outcome in squamous cell carcinoma of the cervix. *Cell Mol Immunol* 2010; **8**: 59–66.
33 Pardoll DM, Topalian SL. The role of CD4+ T cell responses in antitumor immunity. *Curr Opin Immunol* 1998; **10**: 588–94.
34 Huang H, Li F, Gordon JR, Xiang J. Synergistic enhancement of antitumor immunity with adoptively transferred tumor-specific CD4+ and CD8+ T cells and intratumoral lymphotactin transgene expression. *Cancer Res* 2002; **62**: 2043–51.
35 Hung K, Hayashi R, Lafond-Walker A, Lowenstein C, Pardoll D, Levitsky H. The central role of CD4(+) T cells in the antitumor immune response. *J Exp Med* 1998; **188**: 2357–68.
36 Unitt E, Marshall A, Gelson W *et al.* Tumour lymphocytic infiltrate and recurrence of hepatocellular carcinoma following liver transplantation. *J Hepatol* 2006; **45**: 246–53.

37 Cho Y, Miyamoto M, Kato K *et al.* CD4+ and CD8+ T cells cooperate to improve prognosis of patients with esophageal squamous cell carcinoma. *Cancer Res* 2003; **63**: 1555–9.
38 Brunet JF, Dosseto M, Denizot F *et al.* The inducible cytotoxic T-lymphocyte-associated gene transcript CTLA-1 sequence and gene localization to mouse chromosome 14. *Nature* 1986; **322**: 268–71.
39 Jenne DE, Tschopp J. Granzymes, a family of serine proteases released from granules of cytolytic T lymphocytes upon T cell receptor stimulation. *Immunol Rev* 1988; **103**: 53–71.
40 Wahl SM. Transforming growth factor-beta: innately bipolar. *Curr Opin Immunol* 2007; **19**: 55–62.
41 Dooley S, ten Dijke P. TGF-beta in progression of liver disease. *Cell Tissue Res* 2010; **347**: 245–56.
42 Bataller R, Brenner DA. Liver fibrosis. *J Clin Invest* 2005; **115**: 209–18.

Journal of Gastroenterology and Hepatology

JGHF

doi:10.1111/jgh.12484

HEPATOLOGY

Side population cell fractions from hepatocellular carcinoma cell lines increased with tumor dedifferentiation, but lack characteristic features of cancer stem cells

Masamichi Nakayama,*,† Sachiko Ogasawara,* Jun Akiba,* Kosuke Ueda,* Keiko Koura,*,† Keita Todoroki,* Hisafumi Kinoshita† and Hirohisa Yano*

Departments of *Pathology and †Surgery, Kurume University School of Medicine, Kurume, Japan

Key words
cancer stem cells, dedifferentiation, side population cells.

Accepted for publication 15 November 2013.

Correspondence
Dr Jun Akiba, Department of Pathology, Kurume University School of Medicine, 67 Asahimachi, Kurume 830-0011, Japan. E-mail: akiba@med.kurume-u.ac.jp

Abstract

Background and Aim: Cancer stem cells (CSCs), a minority population with stem cell-like characteristics, play important roles in cancer development and progression. Putative CSC markers, such as CD13, CD90, CD133, and epithelial cell adhesion molecule (EpCAM), and side population (SP) technique are generally used in an attempt to isolate CSCs. We aimed to clarify the relationship between CSCs and clonal dedifferentiation in hepatocellular carcinoma (HCC).

Methods: We used a well-differentiated HCC cell line (HAK-1A) and a poorly differentiated HCC cell line (HAK-1B) established from a single nodule with histological heterogeneity. HAK-1B arose because of clonal dedifferentiation of HAK-1A. The SP cells and non-SP (NSP) cells were isolated from the two cell lines with a FACSAria II and used for the analyses.

Results: The SP cell fractions in HAK-1A and HAK-1B were 0.2% and 0.9%, respectively. CD90 or EpCAM was not expressed in either HAK-1A or HAK-1B, while CD13 and CD133 were expressed in HAK-1B alone. Although sphere forming ability, tumorigenicity, growth rate, and CD13 expression were higher in HAK-1B SP cells than HAK-1B NSP cells, there were no differences in drug resistance, colony forming ability, or cell cycle rates between HAK-1B SP and NSP cells, suggesting HAK-1B SP cells do not fulfill CSC criteria.

Conclusions: Our findings suggested a possible relationship between the expression of CSC markers and clonal dedifferentiation. However, the complete features of CSC could not be identified in SP cells, and the concept of SP cells as a universal marker for CSC may not apply to HAK-1A and HAK-1B.

Introduction

Cancer stem cells (CSCs) are defined by self-renewing capacity, differentiation capacity, and tumor-initiating capacity. Additionally, the seeding of metastasis and tumor relapse is attributed to CSCs.[1–3] To date, the existence of CSCs has been proven not only in hematopoietic neoplasms,[4,5] but also various solid neoplasms.[6–11]

Side population (SP) cell sorting was initially applied for the identification of hematopoietic stem cells and has been used to enrich stem cell compartments in diverse tissues and organs.[12–14] SP cells are detected by their ability to efflux Hoechst 33342 dye (Sigma-Aldrich, Saint Louis, MO, USA) through ATP-binding cassette (ABC) membrane transporters. Recently, SP cells have also been used in an attempt to isolate a stem cell-like fraction in cancer cells.[15–17] The approach seems valuable because a variety of cancers, including hepatocellular carcinoma (HCC), highly express ABC transporters, which are reported to contribute to multidrug resistance.[18]

A variety of markers has been successfully used to enrich CSC fractions from different tumors including HCC.[19] Although no markers for putative liver CSCs have been generally accepted, CD133, CD90, epithelial cell adhesion molecule (EpCAM), and CD13 are thought to be candidates for liver CSC markers.[20–24]

Recent evidence suggests that CSCs, a minority population with stem cell-like characteristics, play important roles in cancer development and progression.[25]

In this study, we isolated the SP and non-SP (NSP) cells from two HCC cell lines, a well-differentiated human HCC cell line (HAK-1A) and a poorly differentiated HCC cell line (HAK-1B) which were established from a single nodule with a three-layered structure having different histologic features,[26] and compared the relationship between CSCs and clonal dedifferentiation.

Materials and methods

Cell lines and cell culture. This study used two human HCC cell lines: HAK-1A, HAK-1B, which were both established from a single HCC nodule showing a three-layered structure with a different histological grade in each layer.[26] HAK-1A resembles well-differentiated HCC cells in the outer layer of the original tumor, and HAK-1B resembles poorly differentiated cells in the inner layer. The presence of an identical point mutation in the p53 gene in the two cell lines suggests that they are of clonal origin. The cell culture condition is described elsewhere.[26]

SP cell analysis using flow cytometry. We followed the protocol previously reported by Goodell *et al.*,[13] with minor modifications. Briefly, cells were detached from the culture dish with Accutase (Innovative Cell Technologies, Inc., San Diego, CA, USA). The cells were incubated at 37°C for 60 min with Hoechst 33342 (SIGMA-Aldrich, Saint Louis, MO, USA). The control cells were incubated in the presence of 15 μg Reserpine (SIGMA-Aldrich). After staining, the cells were suspended in phosphate-buffered saline (PBS) with 2% fetal bovine serum (FBS), filtered through a 40-μm cell strainer (BD Biosciences, San Jose, CA, USA). Cells were counterstained with 0.5 μg/mL propidium iodide (PI, BD Biosciences) for the discrimination of dead cells. Viable cells were analyzed and isolated by a FACSAria II (BD Biosciences).

Immunofluorescence flow cytometric analysis of SP and NSP cells. We analyzed SP and NSP cells isolated from HAK-1A and HAK-1B for expression of the putative stem cell markers CD133, CD90, EpCAM, and CD13. Cells were first stained with Hoechst 33342. Excess dye was removed by resuspending 1×10^6 cells/mL in PBS with 2% FBS. Cells were incubated in the dark at 4°C for 30 min with fluorescence-conjugated monoclonal antibodies, including allophycocyanin-conjugated mouse anti human CD133/2 (293C3) antibodies (Miltenyi Biotec, Bergisch-Gladbach, Germany), fluorescein isothiocyanate (FITC)-conjugated mouse anti human CD90, phycoerythrin-conjugated mouse anti-human EpCAM and purified mouse anti-human CD13 (BD Biosciences). After 30 min, cells with purified mouse anti-human CD13 were also incubated in the dark at 4°C for 30 min with goat anti-mouse Ig FITC (BD Biosciences). Cells were counterstained with 0.5 μg/mL PI for the discrimination of dead cells. The data were analyzed using a FACSAria II.

Generation of SP and NSP cells by SP or NSP cells. A total of 1×10^5 sorted SP cells or NSP cells from HAK-1A and HAK-1B were cultured for 1 week, and used for SP cell analysis, as described above, to examine whether SP or NSP cells generate SP and NSP cells.

Proliferation of HAK-1B SP and NSP cells. The proliferative ability of the cells from each subpopulation, including HAK-1B SP and NSP cells, was examined using colorimetric assays with 3-(4, 5-dimethylthiazol-2yl-yl-)-2, 5-dimethyl tetrazolium bromide (MTT) cell growth assay kits (Chemicon, Temecula, CA, USA), as described elsewhere.[27] SP and NSP cells (1500 cells/well) were seeded on 96-well plates (Falcon, Becton Dickinson Labware, Tokyo, Japan) by a FACSAria II. After culture for 24 h, 48 h, 72 h, 96 h, or 120 h, the number of viable cells was examined.

Effects of cisplatin (CDDP), 5-FU, and PEG-IFN-α2b on the proliferation of HAK-1B SP and NSP cells. Effects of CDDP (Nihonkayaku, Tokyo, Japan), 5-fluorouracil (5-FU) (Kyowa Hakko, Tokyo, Japan), and pegylated interferon-α2b (PEG-IFN-α2b) (Schering-Plough K.K., Osaka, Japan) on cell proliferation were examined by MTT assay. SP and NSP cells (1500 cells/well) were seeded on 96-well plates, cultured for 24 h, and then the culture medium was replaced with a new medium containing CDDP alone (0, 0.125, 0.25, or 0.5 μg/mL), 5-FU alone (0, 0.75, 1.5, or 3 μM), or PEG-IFN-α2b (0, 500, 1000, or 2000 IU/mL). After culturing for 48 h or 96 h, the number of viable cells were examined by MTT assay.

Drug treatment assay of SP and NSP cells in HAK-1A and HAK-1B. HAK-1A and HAK-1B cells were cultured with medium alone (control) or medium containing 5-FU (1.5 μM) or PEG-IFN-α2b (1000 IU/mL) and cultured for 96 h, and SP cell analysis, as described above, was performed to estimate the effect of drugs on SP cell fraction.

Cell cycle analysis of HAK-1B SP and NSP cells. Cultured HAK-1B cells were labeled with 10 mM bromodeoxyuridine (Sigma Chemical Co., St. Louis, MO, USA) for 30 min, harvested, and used for the isolation of SP and NSP by a FACSAria II. Isolated SP or NSP cells were used for cell cycle analysis according to the technique described elsewhere.[28] The percentage of the cells in the G_1, S, or G_2/M phase was calculated from a dot plot.

Colony formation assay of HAK-1B SP and NSP cells. Colony formation assay was performed almost according to a modified previously described method.[29] The number of colonies > 0.5 mm in diameter was counted 14 days later.

Sphere formation assay of HAK-1B SP and NSP cells. We performed sphere formation assay according to a previously described method.[29]

Tumorigenicity assay of HAK-1B SP and NSP cells in vivo. Various numbers of cells (1, 5, 10, 50, or 100×10^3) were injected subcutaneously into 4-week-old female NOD/SCID mice ($n = 5$ in each group). Tumorigenic capacity was judged 8 weeks after injection. All procedures were approved by the Ethics Review Committee for Animal Experimentation of Kurume University School of Medicine.

Gene expression microarrays of SP and NSP cells isolated from HAK-1A and HAK-1B. The cRNA was amplified, labeled, and hybridized to a 44 K Agilent 60-mer oligomicroarray according to the manufacturer's instructions. All hybridized microarray slides were scanned by an Agilent scanner. Relative hybridization intensities and background hybridization values were calculated using Agilent Feature Extraction Software (9.5.1.1) (Agilent Technologies, Inc., Santa Clara, CA, USA).

Table 1 Primer and probe mixes list for qRT-PCR analysis

Gene name	Assay IDs
CD13	Hs00174365_m1
CD133	Hs00195682_m1
CD24	Hs03044178_m1
CD44	Hs01075861_m1
CD90	Hs00174816_m1
EpCAM	Hs00158980_m1
ABCG2	Hs01053790_m1
Oct-4	Hs03666771_m1
Nanog	Hs04260366_m1
BMI1	Hs00201350_m1
Alb	Hs00910225_m1
CYP3A4	Hs00604506_m1
β-actin	Hs99999903_m1

Quantitative real-time reverse transcriptase-polymerase chain reaction (qRT-PCR) of SP and NSP cells isolated from HAK-1A and HAK-1B. Total RNA was extracted using RNeasy Plus Micro Kit (Qiagen, Valencia, CA, USA) and complementary DNA (cDNA) was synthesized using Reverse Transcription System (Promega, Madison, WI, USA) according to the manufacturer's instructions. qRT-PCR was carried out with TaqMan technology using ABI PRISM 7500 (Applied Biosystems, Foster City, CA, USA) followed by a previously published method.[29] Gene expression assays primer and probe mixes were used for CD13, CD133, CD24, CD44, CD90, EpCAM, ABCG2, Oct-4, Nanog, BMI1, Alb, CYP3A4, and β-actin (assay IDs are listed in Table 1; Applied Biosystems).

Statistical analysis. Comparison of colorimetric cell growth, drug resistance, colony forming ability, and sphere forming ability were performed using Student's *t*-test. Differences were considered significant at $P < 0.05$.

Results

Identification of SP and NSP cells in HAK-1A and HAK-1B and expression of CSC markers. The SP cell fraction in HAK-1A was very low at only 0.2%. Expression of the putative CSC markers, such as CD133, CD90, EpCAM, CD13, was almost completely absent in both SP and NSP cells from HAK-1A (Fig. 1a). The SP fraction in HAK-1B was 0.9%. Moreover, while CD90 and EpCAM expression was absent in HAK-1B SP and NSP cells, CD133 expression was observed both in 4.6 ~ 6.4% of HAK-1B SP cells and in 3.9 ~ 5.3% of HAK-1B NSP cells. CD13 expression was higher in SP cells (21.7%) than in NSP cells (8.9%) (Fig. 1b).

Generation SP and NSP cells from sorted SP and NSP cells in HAK-1A and HAK-1B. After culturing HAK-1A SP cells or HAK-1B SP cells for 1 week, the percentage of HAK-1A and HAK-1B SP cells decreased to 1.9% and 7.3%, respectively. In contrast, culture of HAK-1A NSP cells and HAK-1B NSP cells generated a small population of SP cells in HAK-1A (0.1%) and HAK-1B (0.7%). The results suggest that the SP cells could generate NSP cells, and vice versa (Fig. 2).

Biological features of SP and NSP cells in HAK-1B cells in vitro. In HAK-1B, SP cell growth was significantly higher than that of NSP cells at every time point (24 h, 48 h, 72 h, 96 h, and 120 h; Fig. 3a). The cell cycle analysis revealed no obvious differences in G_0-G_1/ S/ G_2-M ratios between SP cells (64.0%/ 30.1%/ 4.2%) and NSP cells (65.3%/ 31.9%/ 1.6%) (Fig. 3b).

Drug resistance to 5-FU, CDDP, or PEG-IFN-α2b was examined. The results showed that the viability of HAK-1B SP cells (58.7%) was significantly lower than that of HAK-1B NSP cells (71.5%) at 96 h in cells treated with 0.75 μM 5-FU ($P < 0.001$). Similarly, after 96 h treatment with 1.5 μM 5-FU, viability of SP cells fell to 40.7%, compared with 47.9% in NSP cells ($P < 0.05$). SP cell viability was also significantly lower (50.7%) than NSP cells (63.5%) ($P < 0.05$) after 96 h treatment with 500 IU/mL PEG-IFN-α2b. No other significant differences were observed between SP and NSP cells (Fig. 3c–e). After exposure of HAK-1B cells to PEG-IFN-α2b for 72 h, the percentage of SP cells decreased as compared with control. Conversely, the percentage of SP cells increased when HAK-1B cells were treated with 5-FU for 72 h (Fig. 3f).

In the colony formation assay, SP cells from HAK-1B formed 252 ± 33.4 colonies, while the NSP cells formed 243 ± 70.1 colonies; this difference was not significant (Fig. 4a). Sphere formation was significantly higher in SP cells (21.0 ± 4.1 spheres) as compared with NSP cells (15.7 ± 2.7 spheres) in the HAK-1B cell line ($P < 0.05$; Fig. 4b).

Biological features of SP and NSP cells in HAK-1B cells in vivo. Injection of 1, 5, or 10×10^3 SP or NSP cells produced no tumors in NOD/SCID mice. In contrast, four mice that received 5×10^4 SP cells and five mice that received 10×10^4 SP cells developed tumors at 8 weeks. In addition, one mouse that received 5×10^4 NSP cells and two mice that received 10×10^4 NSP cells also developed small tumors (Fig 4c).

cDNA microarray analysis of gene expression in SP and NSP cells sorted from HAK-1A or HAK-1B cells. cDNA microarray analysis found 884 and 470 differences in gene expression between HAK-1A and HAK-1B, respectively, but there were no significant differences between SP and NSP cells in expression of stemness genes (e.g. CD44, Oct-4, Bim-1, ABCG2, CD24, EpCAM) (Table 2).

qRT-PCR analysis of SP and NSP cells in HAK-1A or HAK-1B cells. SP and NSP cells of HAK-1A and HAK-1B expressed mRNAs of CSC markers, such as CD13, CD133, CD24, CD44, EpCAM, ABCG2, Nanog, and Bmi-1. The expression of these molecules was slightly higher in SP cells than in NSP cells. In addition, the differences in expression levels of CD133, CD24, and CD44 between SP and NSP cells were slightly larger in HAK-1B than HAK-1A cells (Fig. 5a,b). The other putative CSC markers, such as CD90 and Oct-4, were not expressed. As to hepatocyte markers, CYP3A4 was expressed in HAK-1A and HAK-1B, but albumin was not expressed in either cell line.

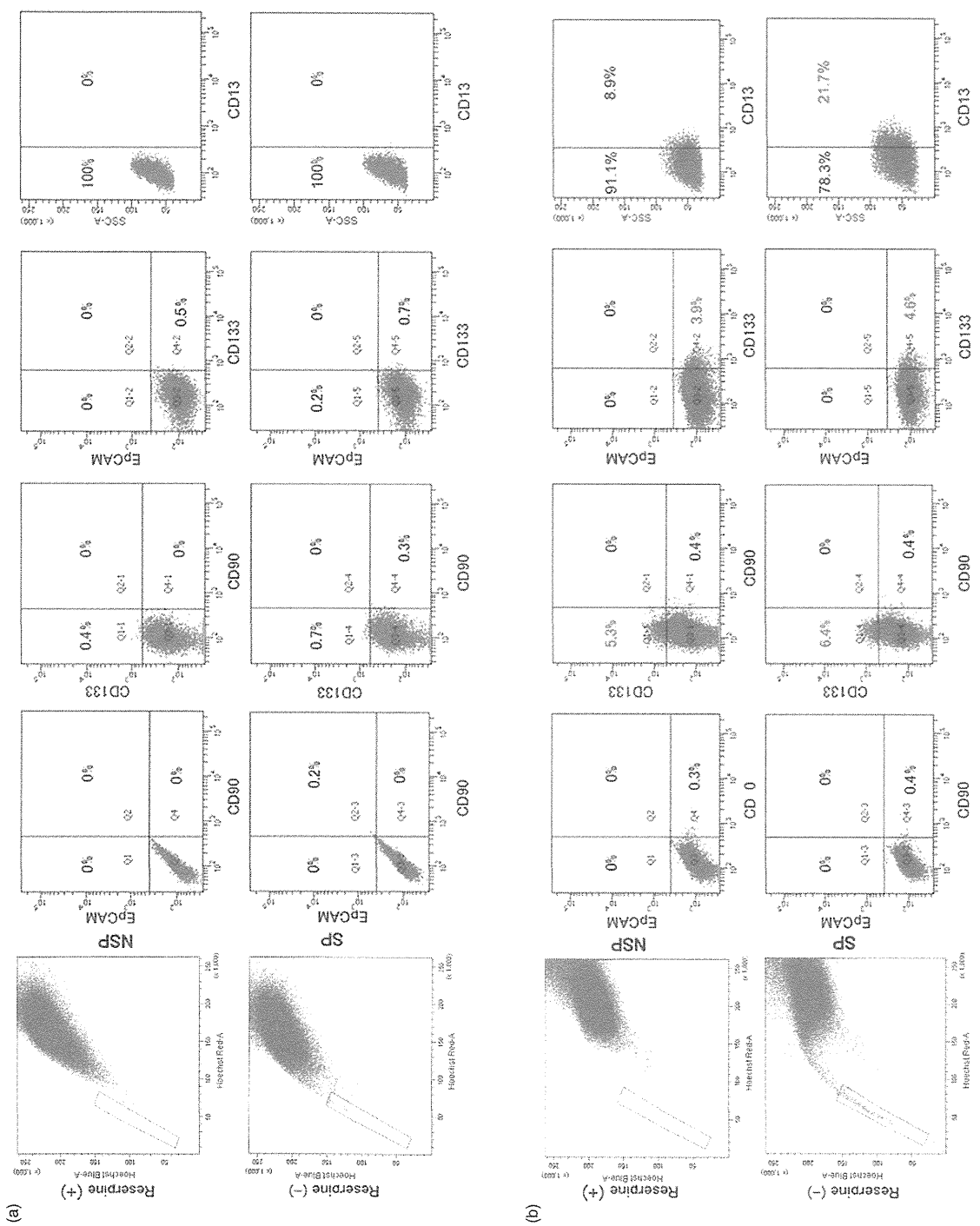

Figure 1 (a) SP cells are considered to be abolished by reserpine. The ratio of SP cells in the HAK-1A cell line was 0.2%. There was almost no expression of CD133, CD90, EpCAM or CD13 in SP and NSP cells from HAK-1A. (b) The ratio of SP cells in the HAK-1B cell line was 0.9%. In the HAK-1B cell line, CD133 was expressed in 4.6 ~ 6.4% of SP cells and 3.9 ~ 5.3% of NSP cells. CD13 expression was higher in SP cells (21.7%) than in NSP cells (8.9%). CD90 and EpCAM expression was low in both SP and NSP cells. The experiments were repeated twice, and almost identical results were obtained.

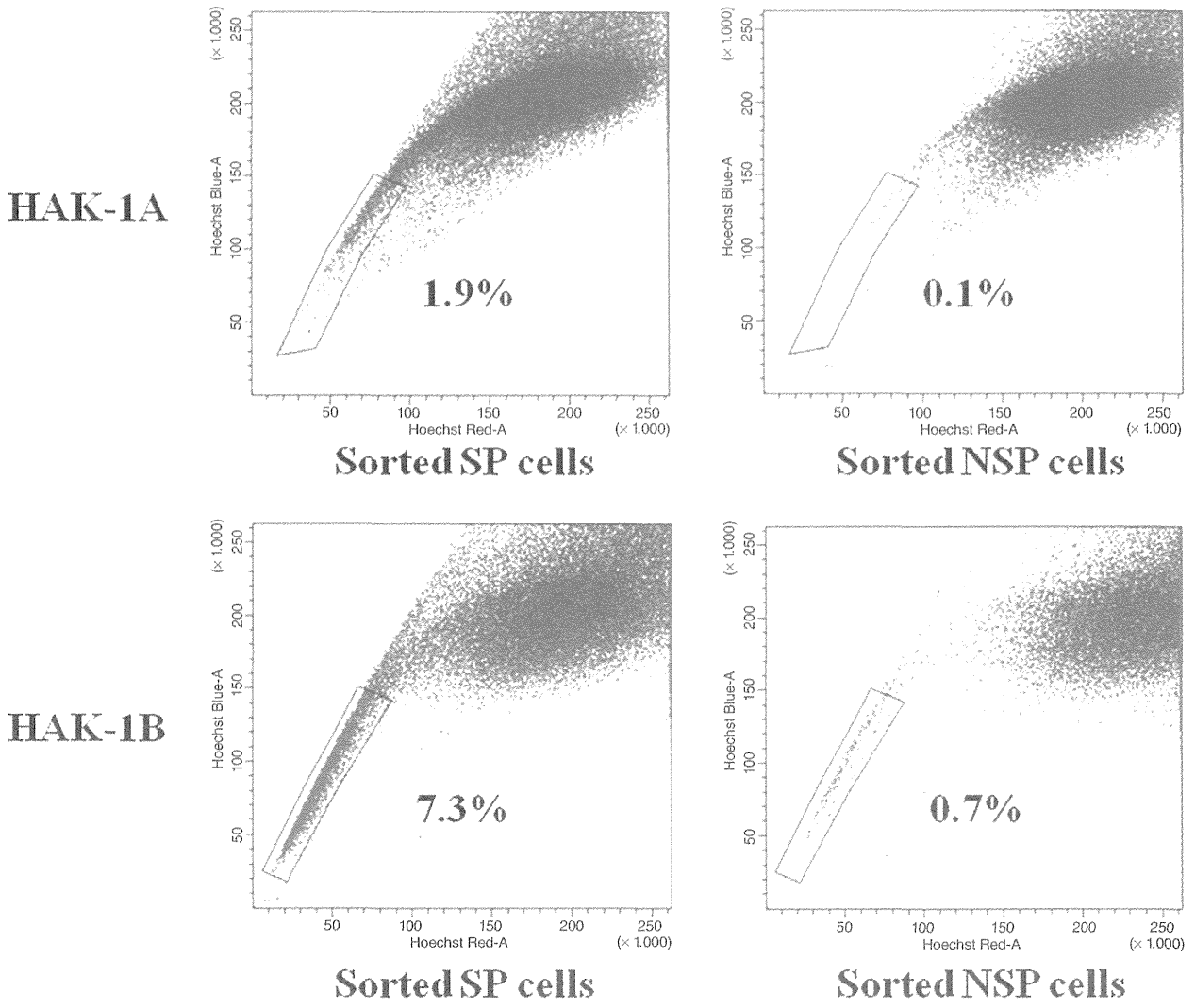

Figure 2 After culturing HAK-1A SP cells or HAK-1B SP cells for 1 week, the percentage of HAK-1A SP cells and HAK-1B SP cells decreased to 1.9% and 7.3%, respectively. In contrast, culture of HAK-1A and HAK-1B NSP cells generated a small population of SP cells in HAK-1A (0.1%) and HAK1B (0.7%). The experiments were repeated twice, and almost identical results were obtained.

Discussion

The present study utilized two HCC cell lines showing clonal dedifferentiation that were established at our department from a single nodule-in-nodule HCC (HAK-1A, HAK-1B), and which are unique in the world. Our aim was to study the SP cell fractions, which are considered universal markers for CSCs,[15–17] in these two cell lines to clarify the relationship between CSCs and clonal dedifferentiation

SP cells from HAK-1A, which was established from a part of the well-differentiated HCC, represented only 0.2% of total cells, an extremely low percentage. However, in SP cells from the HAK-1B cell line, which is a part of the poorly differentiated HCC derived from dedifferentiation of HAK-1A, the SP fraction was 0.9%, 4.5 times higher than in HAK-1A. Further, our analysis of the putative CSCs markers CD133, CD90, EpCAM, and CD13 found no expression of CD90 or EpCAM in either HAK-1A or HAK-1B, while CD13 and CD133 was expressed in HAK-1B alone. In addition, while there was no difference in the expression of CD133 between SP and NSP cells in HAK-1B, CD13 expression was apparently higher in HAK-1B SP cells (21.7%) than HAK-1B NSP cells (8.9%). Haraguchi *et al.*[20] have reported that CD13 was an abundantly expressed marker in SP cells from the HCC cell lines HuH7 and PLC/PRL/5. This fraction existed primarily during the G_0 phase of the cell cycle, and exhibited high tumorigenicity and drug resistance. Our findings suggest the possibility that CD13 could also be a CSC marker for HAK-1B cells. The significance of CD13 in HAK-1B should be further studied.

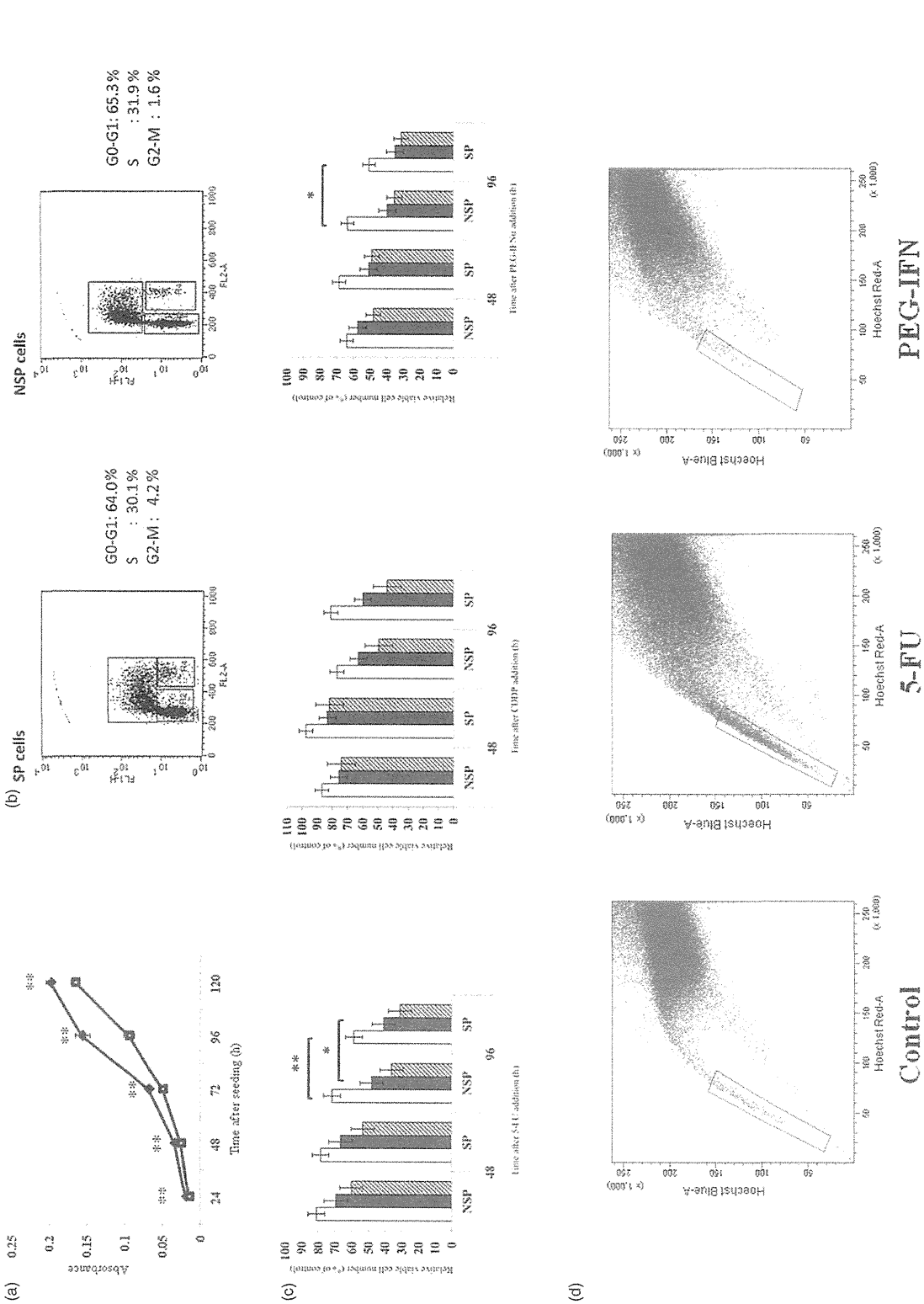

Figure 3 (a) Cell proliferation was significantly higher in SP cells than in NSP cells at 24 h, 48 h, 72 h, 96 h, or 120 h $^{**}P < 0.001$. (♦) SP; (□) NSP. The experiments were repeated twice, and almost identical results were obtained. (b) The cell cycle analysis revealed no obvious differences in G0-G1/ S/ G2-M ratios between SP cells (64.0%/ 30.1%/ 4.2%) and NSP cells (65.3%/ 31.9%/ 1.6%). The experiments were repeated twice, and almost identical results were obtained. (c–e) Drug resistance to CDDP, 5-FU or PEG-IFN-α2b was compared between SP and NSP cells from HAK-1B at 48 h and 96 h. The viability of SP cells was significantly lower than NSP cells after 96 h treatment with 0.75 μM or 1.5 μM 5-FU, or 96 h treatment with 500 IU/mL PEG-IFN-α2b. No other significant differences were observed between SP and NSP cells. $^{*}P < 0.05$, $^{**}P < 0.001$. Figure 3c (□) 0.75 μM 5-FU; (■) 1.5 μM 5-FU; (♦) 3 μM 5-FU. Figure 3d (□) 0.125 μg/ml CDDP; (■) 0.25 μg/ml CDDP; (♦) 0.5 μg/ml CDDP. Figure 3e (□) 500 IU/ml PEG-IFN α2b; (■) 1000 IU/ml PEG-IFN α2b; (■) 2000 IU/ml PEG-IFN α2b. The experiments were repeated at least three times, and almost identical results were obtained. (f) After exposure of HAK-1B cells to PEG-IFN-α2b for 72 h, the percentage of SP cells decreased as compared with control. Conversely, the percentage of SP cells increased when HAK-1B cells were treated with 5-FU for 72 h. The experiments were repeated at least three times, and almost identical results were obtained.

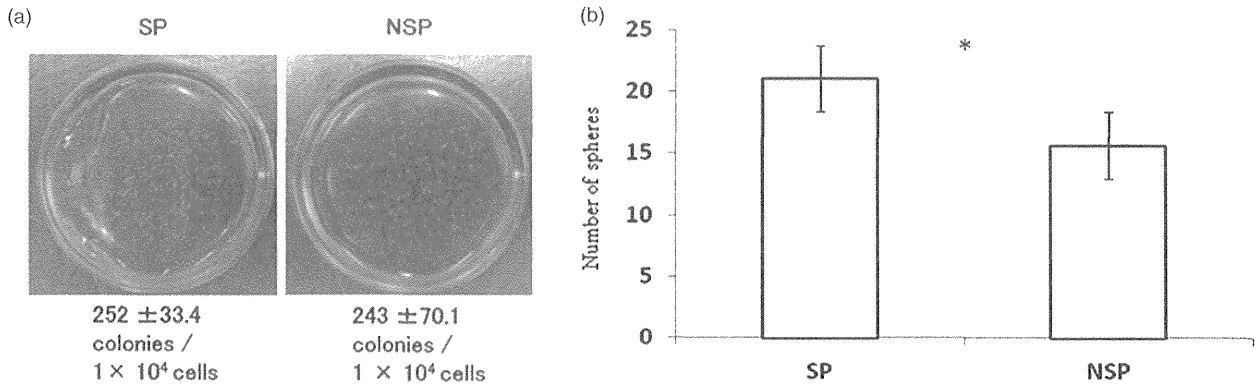

(c)

Tumorigenicity in NOD/SCID mice

Cell type	Injected cell number				
	1,000 cells	5,000 cells	10,000 cells	50,000 cells	100,000 cells
SP	0/5 (0%)	0/5 (0%)	0/5 (0%)	4/5 (80%)	5/5 (100%)
NSP	0/5 (0%)	0/5 (0%)	0/5 (0%)	1/5 (20%)	2/5 (40%)

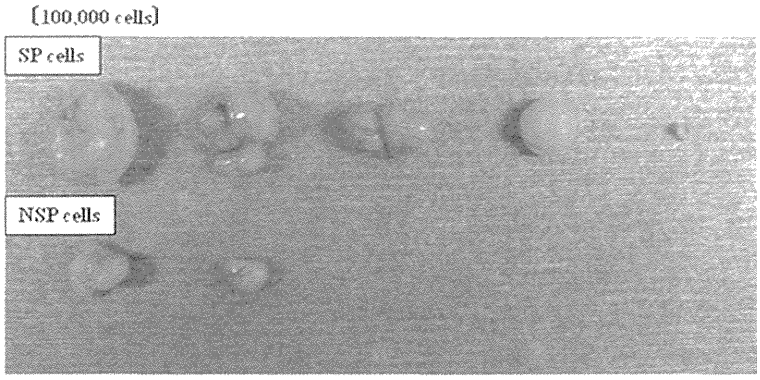

Figure 4 (a) Colony formation assay found no significant difference between HAK-1B SP cells and NSP cells. The experiments were repeated at least three times, and almost identical results were obtained. (b) Sphere formation was significantly higher in HAK-1B SP cells than NSP cells. The experiments were repeated at least three times, and almost identical results were obtained. * $P < 0.05$. (c) Injection of 1, 5, or 10×10^3 SP or NSP cells produced no tumors in NOD/SCID mice. In contrast, four mice that received 5×10^4 SP cells and five mice that received 10×10^4 SP cells developed tumors at 8 weeks. In addition, one mouse that received 5×10^4 NSP cells and two mice that received 10×10^4 NSP cells also developed small tumors.

Analysis of biological features revealed that HAK-1B SP cells possess some properties of CSC, such as higher sphere forming ability and tumorigenicity, as compared with NSP cells. However, HAK-1B SP cells lacked the following four features of CSC. Firstly, HAK-1B SP cells lacked high drug resistance and colony forming ability. Drug treatment usually increases the percentage of CSC, but our results did not always show such tendency, that is PEG-IFN-α2b treatment increased the percentage of SP cells, but 5-FU treatment increased the percentage of SP cells. The reason for this contradictory result is not clear and should be further elucidated. Secondly, the percentage of G_0/G_1 phase is usually higher in CSC, but our cell cycle analysis revealed no difference in rates between SP and NSP cells. Thirdly, differentiated cells do not generate CSC, but in our study, NSP cells could generate SP cells. Fourthly, no difference in microarray analysis and slight difference in qRT-PCR analysis were observed in stemness gene expression between SP and NSP cells.

These results suggest that HAK-1B SP cells do not fulfill the criteria to be considered CSCs.

As described above, it is recognized that the SP cell fraction in a variety of tumors is rich in CSC,[15–17] but some reports question whether there is a relationship between SP cells and CSCs. Burkert

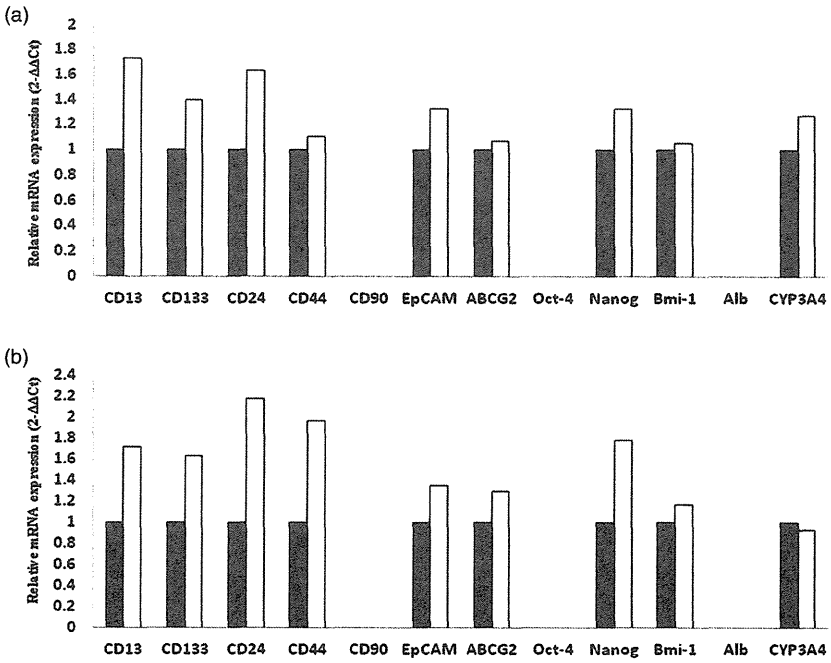

Figure 5 SP and NSP cells of HAK-1A (a) and HAK-1B (b) expressed mRNAs of CSC markers, such as CD13, CD133, CD24, CD44, EpCAM, ABCG2, Nanog, and Bmi-1, and hepatocyte marker, CYP3A4. The expression of CSC markers was slightly higher in SP cells than in NSP cells. (□) SP; (▩) NSP.

Table 2 Summary of cDNA microarray of SP and NSP cells from HAK-1A and HAK-1B

	HAK-1A	HAK-1B
Top Associated Network Functions	RNA Post-Transcription Modification, Cellular Assembly and Organization, DNA Replication, Recombination, and Repair (e.g. ↑FAM124A, C1ORF35, etc.)	Cancer, Drug Metabolism, Molecular Transport (e.g. ↑ALDH3A1, ATF7, IL33, etc.)
Top 5 upregulated molecules in SP versus NSP	GBP5 (× 10.5), BMP3 (× 8.4), SLITRK2 (× 8.1), TMEM90B (× 7.8) CUGBP2 (× 7.6)	FGF2 (× 13.1), ZNF311 (× 12.6), ADH6 (× 8.2), HPCA (× 7.9) AKR1B10 (× 7.6)
Top 5 downregulated molecules in SP versus NSP	ZNF646 (× 11), SAA3P (× 10.1), HTR2C (× 7.5), UGT2B7 (× 7.4), CCR9 (× 7.4)	CACNG3 (× 47.1), HNMT (× 20.3), GAK (× 11.6), C14ORF126 (× 11.5), GGT5 (× 10.7)
Stemness gene expression in SP versus NSP	CD44 (× 1.04), Oct-4 (× 0.95), Bmi-1 (× 0.87), ABCG2 (× 0.83), CD24 (× 0.54), EpCAM (× 1.02)	CD44 (× 0.93), Oct-4 (× 0.84), Bmi-1 (× 0.97), ABCG2 (× 1.47), CD24 (× 1.27), EpCAM (× 0.84)

Gene expression in SP cells and NSP cells sorted from HAK-1A or HAK-1B cells was analyzed by cDNA microarray, but no significant differences were observed between SP cells and NSP cells of either cell line with regard to stemness gene expression.

et al.[30] examined SP and NSP cells in four gastrointestinal cancer cell lines and found that CD34 was expressed in the NSP fraction but not in the SP fraction; however, no significant differences were observed in any other category, including colony formation, tumorigenicity, or multilineage differentiation.

Two main theories are still being debated with regard to the histogenesis of HCC. For many years, the observation of preneoplastic nodules in HCC induced experimentally by exposure to chemicals supported the dedifferentiation hypothesis, that is, the theory that HCC was derived from the dedifferentiation of adult hepatocytes. Further, the recent discovery of the role of small oval cells in the process of carcinogenesis has led to development of the maturation arrest hypothesis, which suggests that HCC derives from the maturation arrest of hepatic stem cells, and analysis of HCC cells has indicated the presence of cells with stem cell-like properties.[31] It is also suspected that dedifferentiation may cause CSCs. As of yet there have been no reports on the relationship between dedifferentiation and CSCs. The present study suggested a relationship between dedifferentiation and expression of CSC markers, but many aspects of the mechanisms of dedifferentiation remain unclear, and many different mechanisms have been reported to explain the abnormal proliferation and dedifferentiation of liver cells in HCC pathogenesis. Among these, the most common are (i) inactivation of p53, p14, and p16; (ii) overexpression of cyclin D1/CDK4, insulin-like growth factor-II or c-MET; or (iii) activation of the Ras/mitogen-activated protein kinase (MAPK), transforming growth factor-β signaling or Wnt/β-catenin signaling.[32–37] Further studies are required to clarify the

mechanisms underlying dedifferentiation, including the relation between dedifferentiation and CSCs.

In conclusion, the present study found that the SP cell fraction was 4.5 times higher in the HAK-1B cell line than in the HAK-1A cell line, and that the expression of CD13 and CD133, which are considered to be CSC markers, was observed only in HAK-1B. Also, a comparison of HAK-1B SP and NSP cells found that CD13 expression was higher in the SP fraction, suggesting a possible relationship between the expression of CSC markers and dedifferentiation. Moreover, HAK-1B SP cells showed more malignant biological features, such as higher sphere forming ability and tumorigenicity as compared with NSP cells. However, with the exception of these biological features, no other CSC characteristics were clearly observed in the HAK-1B SP cells. Thus, the concept of the SP cells as a universal marker for CSC may not apply to HAK-1A and HAK-1B. We plan to examine the relationship between dedifferentiation and CSC using other CSC markers, such as CD13 and CD133.

Acknowledgments

We thank Ms. Akemi Fujiyoshi for her excellent assistance in our experiments.

References

1 Clarke MF, Dick JE, Dirks PB *et al.* Cancer stem cells—perspectives on current status and future directions: AACR Workshop on cancer stem cells. *Cancer Res.* 2006; **66**: 9339–44.
2 Jordan CT, Guzman ML, Noble M. Cancer stem cells. *N. Engl. J. Med.* 2006; **355**: 1253–61.
3 Marquardt JU, Factor VM, Thorgeirsson SS. Epigenetic regulation of cancer stem cells in liver cancer: current concepts and clinical implications. *J. Hepatol.* 2010; **53**: 568–77.
4 Lapidot T, Sirard C, Vormoor J *et al.* A cell initiating human acute myeloid leukaemia after transplantation into SCID mice. *Nature* 1994; **367**: 645–8.
5 Bonnet D, Dick JE. Human acute myeloid leukemia is organized as a hierarchy that originates from a primitive hematopoietic cell. *Nat. Med.* 1997; **3**: 730–7.
6 Collins AT, Berry PA, Hyde C, Stower MJ, Maitland NJ. Prospective identification of tumorigenic prostate cancer stem cells. *Cancer Res.* 2005; **65**: 10946–51.
7 Houghton J, Stoicov C, Nomura S *et al.* Gastric cancer originating from bone marrow-derived cells. *Science* 2004; **306**: 1568–71.
8 Kim CF, Jackson EL, Woolfenden AE *et al.* Identification of bronchioalveolar stem cells in normal lung and lung cancer. *Cell* 2005; **121**: 823–35.
9 Ponti D, Costa A, Zaffaroni N *et al.* Isolation and in vitro propagation of tumorigenic breast cancer cells with stem/progenitor cell properties. *Cancer Res.* 2005; **65**: 5506–11.
10 Ricci-Vitiani L, Lombardi DG, Pilozzi E *et al.* Identification and expansion of human colon-cancer-initiating cells. *Nature* 2007; **445**: 111–5.
11 Singh SK, Clarke ID, Terasaki M *et al.* Identification of a cancer stem cell in human brain tumors. *Cancer Res.* 2003; **63**: 5821–8.
12 Falciatori I, Borsellino G, Haliassos N *et al.* Identification and enrichment of spermatogonial stem cells displaying side-population phenotype in immature mouse testis. *FASEB J.* 2004; **18**: 376–8.
13 Goodell MA, Brose K, Paradis G, Conner AS, Mulligan RC. Isolation and functional properties of murine hematopoietic stem cells that are replicating in vivo. *J. Exp. Med.* 1996; **183**: 1797–806.
14 Shimano K, Satake M, Okaya A *et al.* Hepatic oval cells have the side population phenotype defined by expression of ATP-binding cassette transporter ABCG2/BCRP1. *Am. J. Pathol.* 2003; **163**: 3–9.
15 Kondo T, Setoguchi T, Taga T. Persistence of a small subpopulation of cancer stem-like cells in the C6 glioma cell line. *Proc. Natl Acad. Sci. U.S.A.* 2004; **101**: 781–6.
16 Chiba T, Kita K, Zheng YW *et al.* Side population purified from hepatocellular carcinoma cells harbors cancer stem cell-like properties. *Hepatology* 2006; **44**: 240–51.
17 Patrawala L, Calhoun T, Schneider-Broussard R, Zhou J, Claypool K, Tang DG. Side population is enriched in tumorigenic, stem-like cancer cells, whereas ABCG2+ and ABCG2- cancer cells are similarly tumorigenic. *Cancer Res.* 2005; **65**: 6207–19.
18 Itsubo M, Ishikawa T, Toda G, Tanaka M. Immunohistochemical study of expression and cellular localization of the multidrug resistance gene product P-glycoprotein in primary liver carcinoma. *Cancer* 1994; **73**: 298–303.
19 Park CY, Tseng D, Weissman IL. Cancer stem cell-directed therapies: recent data from the laboratory and clinic. *Mol. Ther.* 2009; **17**: 219–30.
20 Haraguchi N, Ishii H, Mimori K *et al.* CD13 is a therapeutic target in human liver cancer stem cells. *J. Clin. Invest.* 2010; **120**: 3326–39.
21 Ma S, Chan KW, Hu L *et al.* Identification and characterization of tumorigenic liver cancer stem/progenitor cells. *Gastroenterology* 2007; **132**: 2542–56.
22 Suetsugu A, Nagaki M, Aoki H, Motohashi T, Kunisada T, Moriwaki H. Characterization of CD133+ hepatocellular carcinoma cells as cancer stem/progenitor cells. *Biochem. Biophys. Res. Commun.* 2006; **351**: 820–4.
23 Yamashita T, Ji J, Budhu A *et al.* EpCAM-positive hepatocellular carcinoma cells are tumor-initiating cells with stem/progenitor cell features. *Gastroenterology* 2009; **136**: 1012–24.
24 Yang ZF, Ho DW, Ng MN *et al.* Significance of CD90+ cancer stem cells in human liver cancer. *Cancer Cell* 2008; **13**: 153–66.
25 Libbrecht L. Hepatic progenitor cells in human liver tumor development. *World J. Gastroenterol.* 2006; **12**: 6261–5.
26 Yano H, Iemura A, Fukuda K, Mizoguchi A, Haramaki M, Kojiro M. Establishment of two distinct human hepatocellular carcinoma cell lines from a single nodule showing clonal dedifferentiation of cancer cells. *Hepatology* 1993; **18**: 320–7.
27 Hisaka T, Yano H, Ogasawara S *et al.* Interferon-alphaCon1 suppresses proliferation of liver cancer cell lines in vitro and in vivo. *J. Hepatol.* 2004; **41**: 782–9.
28 Yano H, Iemura A, Haramaki M *et al.* Interferon alfa receptor expression and growth inhibition by interferon alfa in human liver cancer cell lines. *Hepatology* 1999; **29**: 1708–17.
29 Ueda K, Ogasawara S, Akiba J *et al.* Aldehyde dehydrogenase 1 identifies cells with cancer stem cell-like properties in a human renal cell carcinoma cell line. *PLOS ONE* 2013; **8**: e75463.
30 Burkert J, Otto WR, Wright NA. Side populations of gastrointestinal cancers are not enriched in stem cells. *J. Pathol.* 2008; **214**: 564–73.
31 Sell S, Leffert HL. Liver cancer stem cells. *J. Clin. Oncol.* 2008; **26**: 2800–5.
32 Breuhahn K, Longerich T, Schirmacher P. Dysregulation of growth factor signaling in human hepatocellular carcinoma. *Oncogene* 2006; **25**: 3787–800.
33 El-Serag HB, Rudolph KL. Hepatocellular carcinoma: epidemiology and molecular carcinogenesis. *Gastroenterology* 2007; **132**: 2557–76.

34 Tannapfel A, Busse C, Weinans L *et al.* INK4a-ARF alterations and p53 mutations in hepatocellular carcinomas. *Oncogene* 2001; **20**: 7104–9.
35 Teufel A, Staib F, Kanzler S, Weinmann A, Schulze-Bergkamen H, Galle PR. Genetics of hepatocellular carcinoma. *World J. Gastroenterol.* 2007; **13**: 2271–82.
36 van Zijl F, Zulehner G, Petz M *et al.* Epithelial-mesenchymal transition in hepatocellular carcinoma. *Future Oncol.* 2009; **5**: 1169–79.
37 Villanueva A, Newell P, Chiang DY, Friedman SL, Llovet JM. Genomics and signaling pathways in hepatocellular carcinoma. *Semin. Liver Dis.* 2007; **27**: 55–76.

nature nanotechnology

LETTERS

PUBLISHED ONLINE: 5 OCTOBER 2014 | DOI: 10.1038/NNANO.2014.208

Self-assembled micellar nanocomplexes comprising green tea catechin derivatives and protein drugs for cancer therapy

Joo Eun Chung[1†*], Susi Tan[1†], Shu Jun Gao[1], Nunnarpas Yongvongsoontorn[1], Soon Hee Kim[2], Jeong Heon Lee[2], Hak Soo Choi[2], Hirohisa Yano[1,3], Lang Zhuo[1], Motoichi Kurisawa[1*] and Jackie Y. Ying[1]

When designing drug carriers, the drug-to-carrier ratio is an important consideration, because the use of high quantities of carriers can result in toxicity as a consequence of poor metabolism and elimination of the carriers[1]. However, these issues would be of less concern if both the drug and carrier had therapeutic effects. (−)-Epigallocatechin-3-*O*-gallate (EGCG), a major ingredient of green tea, has been shown, for example, to possess anticancer effects[2–7], anti-HIV effects[8], neuroprotective effects[9] and DNA-protective effects[10]. Here, we show that sequential self-assembly of the EGCG derivative with anticancer proteins leads to the formation of stable micellar nanocomplexes, which have greater anticancer effects *in vitro* and *in vivo* than the free protein. The micellar nanocomplex is obtained by complexation of oligomerized EGCG with the anticancer protein Herceptin to form the core, followed by complexation of poly(ethylene glycol)–EGCG to form the shell. When injected into mice, the Herceptin-loaded micellar nanocomplex demonstrates better tumour selectivity and growth reduction, as well as longer blood half-life, than free Herceptin.

Many macromolecular drug carriers have been significantly improved to alter the pharmacokinetics and biodistribution of drugs[11–23], but the carrier is still just an excipient for drug delivery and only the drug is the therapeutically relevant compound. We were inspired to design an improved delivery system in which the carrier would also display therapeutic effects. This was achieved by utilizing the binding property of (−)-epigallocatechin-3-*O*-gallate (EGCG) with various biological molecules including proteins[24,25]. We synthesized a micellar nanocomplex (MNC) carrier comprising two EGCG derivatives designed to bind with proteins in a spatially ordered structure. One of them was oligomerized EGCG (OEGCG), which was designed to stabilize the core by strengthening the binding property of EGCG with the proteins[26]. The other derivative was poly(ethylene glycol)–EGCG (PEG–EGCG), which was tailored to bind with the protein/OEGCG complex as an inert and hydrophilic shell with extended PEG chains. The MNCs were formed via two sequential self-assembly steps in aqueous solution: (1) complexation between OEGCG and proteins to form the core and (2) complexation of the PEG–EGCG surrounding the pre-formed core to form the shell (Fig. 1a). The micellar structure, with its PEG shell, could reduce protein immunogenicity and prevent rapid renal clearance and proteolysis of the protein, decreasing the need for frequent injections or infusion therapy[16,21]. Although many studies have discussed the beneficial bioactivities of EGCG, here we have attempted to utilize EGCG as a carrier for biological molecules, aiming to achieve combinational therapeutic effects between the carrier and the drug.

OEGCG and PEG–EGCG were synthesized by the Baeyer reaction between an aldehyde group and a nucleophilic A ring of the EGCG[27] (Supplementary Figs 1–3). PEG–EGCG and OEGCG showed no and low cytotoxicity, respectively, on human normal mammary epithelial cells (HMECs) in the range of concentrations tested, but they showed substantial cancer cell growth inhibitory effects on a HER2-overexpressing human breast cancer cell line (BT-474) in a concentration-dependent manner (Supplementary Fig. 4).

Figure 1b,c presents transmission electron microscopy (TEM) images (Fig. 1b) and hydrodynamic diameters (HDs; Fig. 1c) of the complexes formed at each step of the two sequential self-assemblies, respectively. Herceptin (a trade name for the drug trastuzumab), which is a humanized monoclonal antibody against the HER2/neu (erbB2) receptor that induces regression of HER2-overexpressing metastatic breast cancer tumours, has an HD of ~9 nm. Adding OEGCG to the Herceptin solution led to the spontaneous formation of a complex with a relatively broad size distribution. Indeed, the TEM image of the Herceptin/OEGCG complex shows a varied degree of complex association. Subsequent addition of PEG–EGCG to the Herceptin/OEGCG complexes led to the formation of monodispersed spherical complexes (HD ≈ 90 nm).

The complexation of OEGCG and Herceptin was explored using dynamic light scattering and varying the concentration of each component (Fig. 2a). The size of complex formed increased with increasing OEGCG concentration when the protein concentration was held constant. However, when the Herceptin concentration was increased while keeping the OEGCG concentration constant, the complex size increased up to a maximum, followed by a decrease with a further increase in Herceptin concentration. This indicates that the OEGCG complexes with Herceptin via non-covalent bonds. To investigate the interaction in this complexation, Tween 20, Triton X-100, sodium dodecyl sulphate (SDS), urea and NaCl were added to the complex (Fig. 2b). Complexes were effectively dissociated by Tween 20, Triton X-100 and SDS as a result of hydrophobic competition. In contrast,

[1]Institute of Bioengineering and Nanotechnology, 31 Biopolis Way, The Nanos, 138669 Singapore, [2]Division of Hematology/Oncology, Department of Medicine, Beth Israel Deaconess Medical Center and Harvard Medical School, 330 Brookline Avenue, Boston, Massachusetts 02215, USA, [3]Department of Pathology, Kurume University School of Medicine, 67 Asahi-machi, 830-0011 Kurume, Japan, †These authors contributed equally to this work.
*e-mail: jechung@ibn.a-star.edu.sg; mkurisawa@ibn.a-star.edu.sg

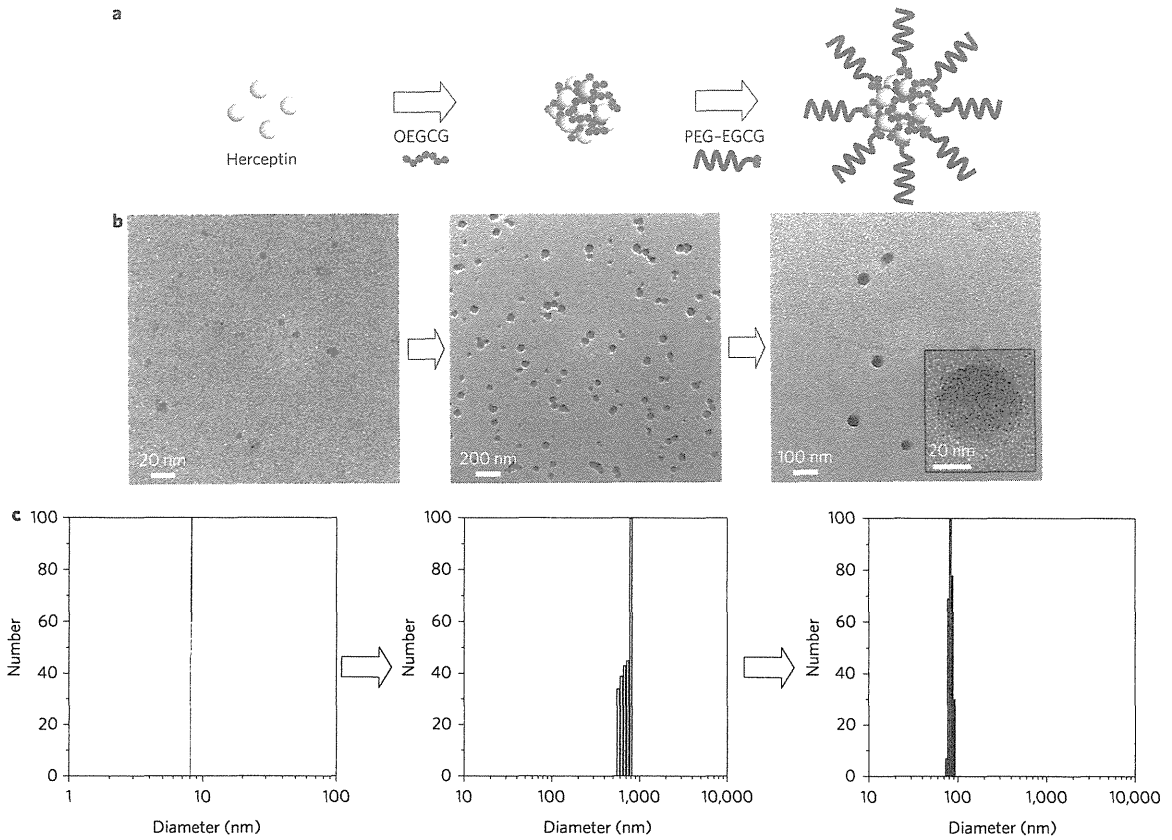

Figure 1 | Schematic diagram and morphology of self-assembled MNCs loaded with proteins. a, Schematic of the self-assembly process used to form the MNCs, which are formed via two sequential self-assemblies in an aqueous solution: complexation of OEGCG with proteins to form the core, followed by complexation of PEG-EGCG surrounding the pre-formed core to form the shell. **b**,**c**, TEM images (**b**) and hydrodynamic size distributions (**c**) of complexes observed at each step of self-assembly. In the inset in the right-most panel in **b**, a high-magnification image shows a single MNC.

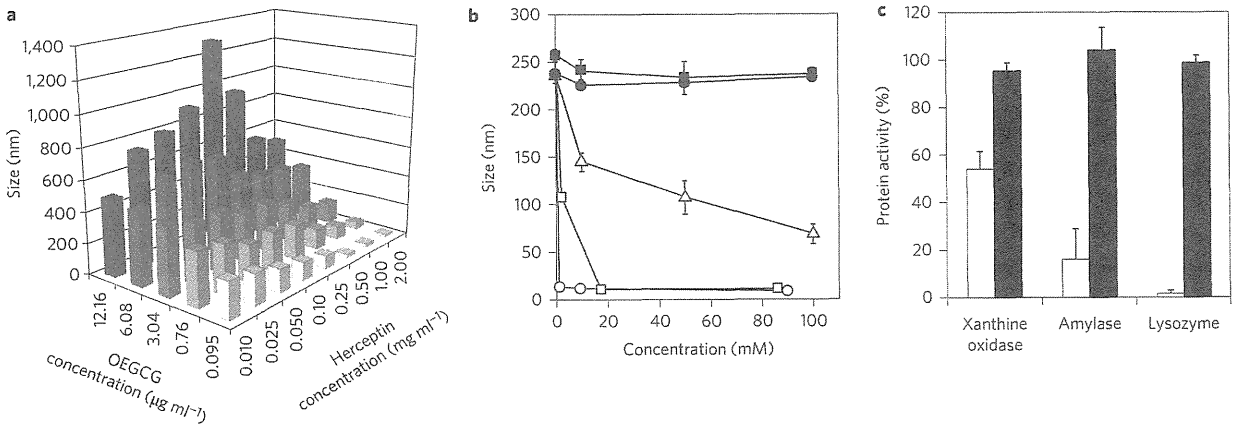

Figure 2 | Formation and dissociation of protein/OEGCG complexes. a, Size of Herceptin/OEGCG complexes formed with different concentrations of OEGCG and Herceptin. The data indicate that OEGCG complexes with Herceptin via non-covalent bonds. Results are reported as mean values ($n = 3$). **b**, Complex dissociation by Tween 20 (open circles), Triton X-100 (open squares), SDS (open triangles), urea (filled circles) and NaCl (filled squares). Complexes were effectively dissociated by Tween 20, Triton X-100 and SDS due to hydrophobic competition, demonstrating that the dominant mode of interaction between OEGCG and the proteins is a hydrophobic interaction ($n = 3$, mean ± s.d.). **c**, Protein activities were restrained by complexation with OEGCG (open bars) and fully restored by dissociation (filled bars) (protein/OEGCG wt/wt ratio = 1). Triton X-100 (0.1%) was used as a dissociator ($n = 3$, mean ± s.d.).

urea (which has the ability to participate in the formation of strong hydrogen bonds and is not intrinsically hydrophobic) and NaCl were ineffective in dissociating the complexes. These results illustrate that the dominant mode of interaction between OEGCG and proteins is a hydrophobic interaction, rather than hydrogen bonding or an ionic interaction.